ACS APPLIED NANO MATERIALS

www.acsanm.org Article

Room-Temperature Large-Scale Synthesis of Black-Phase $CsPbI_3$ Nanocrystals for Red Light-Emitting Diodes

Ju-Hyun Yoo, Kyung Yeon Jang, Jihye Jang, Cheolmin Park, Tae-Woo Lee, and Jin-Woo Park*

Cite This: https://doi.org/10.1021/acsanm.4c04001 Read Online

ACCESS | Metrics & More | Article Recommendations | Supporting Information

ABSTRACT: Inorganic perovskite nanocrystals (IPNCs) are gaining attention as next-generation luminescent materials due to their excellent optoelectronic properties and thermal stability. However, current challenges in achieving large-scale synthesis hinder quality improvement and their commercialization. In particular, $CsPbI_3$, which exhibits red emission, stabilizes in a nonradiative yellow phase at room temperature, making it difficult to synthesize the radiative black phase under ambient conditions. Currently, the synthesis of IPNCs is limited to small-scale laboratory procedures. In response to the demand for stable room-temperature synthesis methods of $CsPbI_3$ and the need for large-scale synthesis of IPNCs, we present large-scale synthesis of black-phase $CsPbI_3$ nanocrystals at room temperature by starting from nanostructures and adjusting the Cs-to-Pb ratio to prevent the formation of yellow-phase $CsPbI_3$. The probability of cesium occupying the A site in the perovskite structure (ABX_3) varies with the Cs-to-Pb ratio, leading to differences in the growth rate of the nanocrystals. By adjusting the amount of oleylammonium on the surface of the $CsPbI_3$ nanocrystals, we controlled the synthesis process. As a result, we achieved a photoluminescence quantum yield (PLQY) of 72% at 670 nm by synthesizing $CsPbI_3$ nanocrystals in a 1 L bottle, utilizing more than 800 times the compound quantity compared to laboratory-scale methods. Furthermore, we fabricated red light-emitting diodes (LEDs) with an external quantum efficiency of 6.4% and a full width at half-maximum (fwhm) of 33 nm. This room-temperature large-scale synthesis method for $CsPbI_3$ nanocrystals holds significant promise for the future commercialization of inorganic perovskite LEDs.

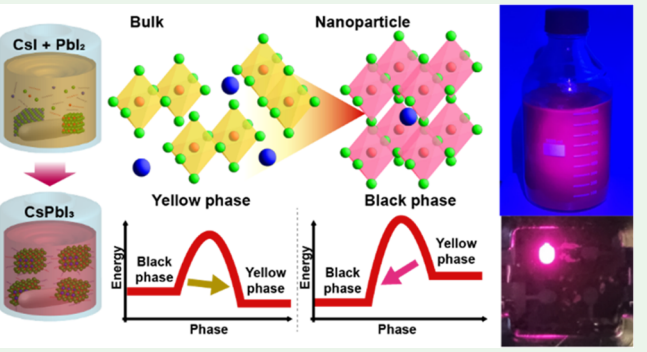

KEYWORDS: *cesium lead iodide, perovskite nanocrystals, large-scale synthesis, room-temperature synthesis, red light-emitting diodes*

INTRODUCTION

Recently, inorganic halide perovskite nanocrystals (IPNCs) have been extensively studied because of their higher thermal stability than organic−inorganic hybrid halide perovskite nanocrystals.[1−7] IPNCs possess superior properties such as easily adjusting the bandgap by changing the proportion of the constituent elements or morphology, narrow full width at half-maximum (fwhm), high photoluminescence quantum yield (PLQY), solution processability, and ease of synthesis.[8−12] These excellent photoelectric properties of IPNCs can be used for light-emitting diodes (LEDs), solar cells, photodetectors, and lasers.[3,10,13−16]

Commercializing IPNCs requires not only improving the performance of IPNCs but also developing technology for their large-scale synthesis.[17] Because it is crucial to reduce the cost for large-scale synthesis, securing room-temperature synthetic technology and minimizing the synthesis steps are necessary.[18] However, currently, synthesis is primarily conducted on a small scale in laboratory settings, typically in a high-temperature inert gas environment.[19] Although room-temperature synthesis is possible, the synthesis of IPNCs is not efficient, and show low PLQY.[20] Therefore, for the commercialization of IPNCs, the development of a large-scale synthesis method is essential.[17] In this work, large-scale synthesis refers to synthesizing more than 500 times the typical amount (0.04 mmol), with the ultimate goal being a method that allows uniform synthesis regardless of the quantity.

Unlike green IPNCs, red and blue IPNCs are hard to mass-synthesize at room temperature. For blue IPNCs, the low solubility of the compounds makes them challenging to synthesize at room temperature, and a mixture of Br^- and Cl^- causes ion migration, which causes phase separation and redshift.[21,22] In our previous study, we developed a room-temperature one-pot synthesis method and solved this problem by synthesizing $CsPbBr_3$ nanoplatelets without using Cl^-.[18]

Received: July 12, 2024
Revised: November 25, 2024
Accepted: November 28, 2024

https://doi.org/10.1021/acsanm.4c04001
ACS Appl. Nano Mater. XXXX, XXX, XXX−XXX

However, it is still hard to mass-synthesize red IPNCs at room temperature.[23] The blue and green perovskite structures using Br^- and Cl^- satisfy the Goldschmidt tolerance factor, but the Goldschmidt tolerance factor of $CsPbI_3$—which is used for red IPNCs—is slightly out of the stable range for the perovskite structure.[10,11] Therefore, $CsPbI_3$ exists in a black phase (α-cubic, β-tetragonal, and γ-orthorhombic), which is a perovskite structure having light-emitting properties, and a yellow phase (δ-orthorhombic), which is not a perovskite structure and has no light-emitting properties.[10,11,24−27] Because the yellow phase (a nonperovskite structure) is more stable at room temperature, there are few methods to synthesize the black phase at room temperature.[2,11,14,19,24−26]

To date, two primary methods have been used to synthesize IPNCs: (1) the hot-injection (HI) method and (2) the ligand-assisted reprecipitation (LARP) method.[19,20] The HI method is unsuitable for large-scale synthesis because it undergoes several process steps, such as high-temperature control, maintaining an inert gas atmosphere, and complex precursor preparation.[8,14,19,28] The LARP method is processed at room temperature, and a polar solvent such as *N*,*N*-dimethylformamide (DMF) or dimethyl sulfoxide (DMSO) is used during the reaction.[8,9,29] However, polar solvents cause a phase transition of $CsPbI_3$ to a yellow phase, making them unsuitable for synthesizing $CsPbI_3$.[8,9,11,30] Furthermore, both the HI and LARP methods include steps for mixing different solutions. Since the reaction begins immediately after mixing, in large-scale synthesis, the reaction starts before the solutions are evenly mixed.[8] Therefore, it is challenging to mass-synthesize IPNCs using the HI and LARP methods.[8,9,23]

Wang et al. and Huang et al. synthesized $CsPbI_3$ nanocrystals at room temperature.[9,23] However, their methods still require precursor preparation and mixing steps or require a heating process under certain conditions.[9,23] The precursor mixing step hinders homogeneous large-scale synthesis because it is difficult to mix evenly before the reaction when synthesizing a large amount.[8,9,23] Therefore, in large-scale room-temperature synthesis method of $CsPbI_3$ into the black phase, there should be no solution-mixing step or a reaction should start after evenly mixed.

In this study, $CsPbI_3$ nanocrystals are mass-synthesized at room temperature without a solution-mixing step based on our previous research, a large-scale synthesis method for blue inorganic perovskite nanoplatelets.[18] $CsPbI_3$ is stable as a yellow phase at room temperature.[11,26,31] However, we used the property that the black phase becomes more stable than the yellow phase when the size of $CsPbI_3$ nanoparticles is reduced to smaller than 5.6 nm.[32] After synthesizing them into nanoparticles to sizes below 5.6 nm, we slowly grew the size of the nanoparticles.

Afterward, even though the yellow phase becomes more stable than the black phase, in the nanoparticles, the activation energy for a phase transition is higher than bulk, so nanoparticles are not readily transformed to the yellow phase.[33,34] Furthermore, adjusting the ratio of Cs to Pb made it possible to synthesize a stable black phase.[35] In addition, we monitored the phase transition of the synthesized nanocrystals over time and adjusted their growth rate by varying the amount of oleylamine. We synthesized $CsPbI_3$ nanocrystals with a PLQY of 72% at a 670 nm emission peak using this large-scale synthesis method. The quantity of PbI_2 used in the synthesis is 32 mmol, which is more than 800 times the typical amount used in a single synthesis (typically 0.04 mmol or less).[19,20] The mechanism and phase transitions depending on the synthesis time of the $CsPbI_3$ nanocrystals were observed using high-resolution transmission electron microscopy (TEM) and high-resolution X-ray diffraction (XRD). The luminescent properties of the nanocrystals were analyzed through photoluminescence (PL) and electroluminescence (EL) spectra.

EXPERIMENTAL SECTION

Materials. Cesium iodide (CsI, 99.9%), lead iodide (PbI_2, 99%), oleic acid (OA, 90%), oleylamine (OAm, 70%), cyclohexane (99.5%), hexane (95%), ethyl acetate (99.8%), *N*,*N*-dimethylformamide (DMF), dimethyl sulfoxide (DMSO), 4-dodecylbenzenesulfonic acid (DBSA), poly-TPD ($M_n \geq 20{,}000$) and chlorobenzene (99.8%) were purchased from Sigma−Aldrich. Toluene, acetone, and IPA were purchased from Duksan Pure Chemical. Poly(2,3-dihydrothieno-1,4-dioxin)-poly(styrenesulfonate) (PEDOT:PSS, AI 4083) was purchased from Heraeus.

Synthesis of Nanocrystals. A total of 1.2 mmol of CsI and 0.4 mmol of PbI_2 were loaded into a 20 mL vial, and 10 mL of toluene, 1 mL of OA, and 0.49 mL of OAm were added. The solution was then stirred at 300 rpm at room temperature for 72 h. At the end of stirring, the solution was centrifuged with several steps to separate the nanocrystals. First, the obtained solution was centrifuged at 12,000 rpm for 5 min to remove the ligands and unreacted chemicals. The supernatant was discarded, and the precipitate was redispersed in cyclohexane. Then, the IPNCs in solution were centrifuged at 8000 rpm for 3 min to remove the large particles. The precipitate was discarded, and ethyl acetate was added in a 1:1 ratio to the supernatant. Then, the IPNCs in solution were centrifuged at 12,000 rpm for 5 min to wash out the ligands. The precipitate was collected and redispersed in hexane.

Large-Scale Synthesis of Nanocrystals. Large-scale synthesis was performed by increasing the precursors used in small-scale syntheses. A total of 96 mmol of CsI and 32 mmol of PbI_2 were loaded into a 1 L bottle, and 800 mL of toluene, 80 mL of OA, and 39.2 mL of OAm were added. The solution was then stirred at 300 rpm at room temperature for 72 h. At the end of stirring, the solution was centrifuged with several steps to separate the nanocrystals. First, the obtained solution was centrifuged at 12,000 rpm for 5 min to remove the ligands and unreacted chemicals. The supernatant was discarded, and the precipitate was redispersed in cyclohexane. Then, the IPNCs in solution were centrifuged at 8000 rpm for 3 min to remove the large particles. The precipitate was discarded, and ethyl acetate was added in a 1:1 ratio to the supernatant. Then, the IPNCs in solution were centrifuged at 12,000 rpm for 5 min to wash out the ligands. The precipitate was collected and redispersed in hexane.

ZnI_2 Post-Treatment. ZnI_2 (0.3 mmol) was loaded into a vial, and 10 mL of hexane and 0.2 mL of OAm were added. The solution was then stirred at 300 rpm for 24 h. We added ZnI_2 solution to the synthesized $CsPbI_3$ solution.

Device Fabrication. A 2.5 cm × 2.5 cm glass was washed via sequential ultrasonication in acetone, IPA, and deionized water for 5 min each. Patterned ITO was deposited 100 nm thick on the glass using a direct current magnetron sputter. The ITO-deposited glass was oxygen plasma-treated at 140 W for 90 s. On the ITO-deposited glass, the HTL solution (1:1 PEDOT:PSS and IPA) was spin-coated at 4000 rpm for 60 s and annealed at 130 °C for 20 min. Then, poly-TPD solution (10 mg/mL, chlorobenzene) was spin-coated at 4000 rpm for 45 s on the HTL in a nitrogen-filled glovebox and annealed at 120 °C for 10 min. The obtained nanocrystal solution was spin-coated at 2000 rpm for 60 s in a nitrogen-filled glovebox. A 45 nm thick TPBi layer, 1 nm thick LiF layer, and 100 nm thick Al layer were sequentially deposited on the emitting layer using a thermal evaporator.

Characterization. PL emission spectra and PLQYs were collected with a Jasco FP-8500 spectrofluorometer. Absorption spectra were measured with a ultraviolet−visible (UV−vis) spectrometer. TEM images were obtained with a JEM-ARM 200F NEOARM (JEOL). XRD measurements were performed with a SmartLab system (Rigaku). The EL spectrum of the device was measured using a spectroradiometer (Konica, CS 2000).

https://doi.org/10.1021/acsanm.4c04001
ACS Appl. Nano Mater. XXXX, XXX, XXX−XXX

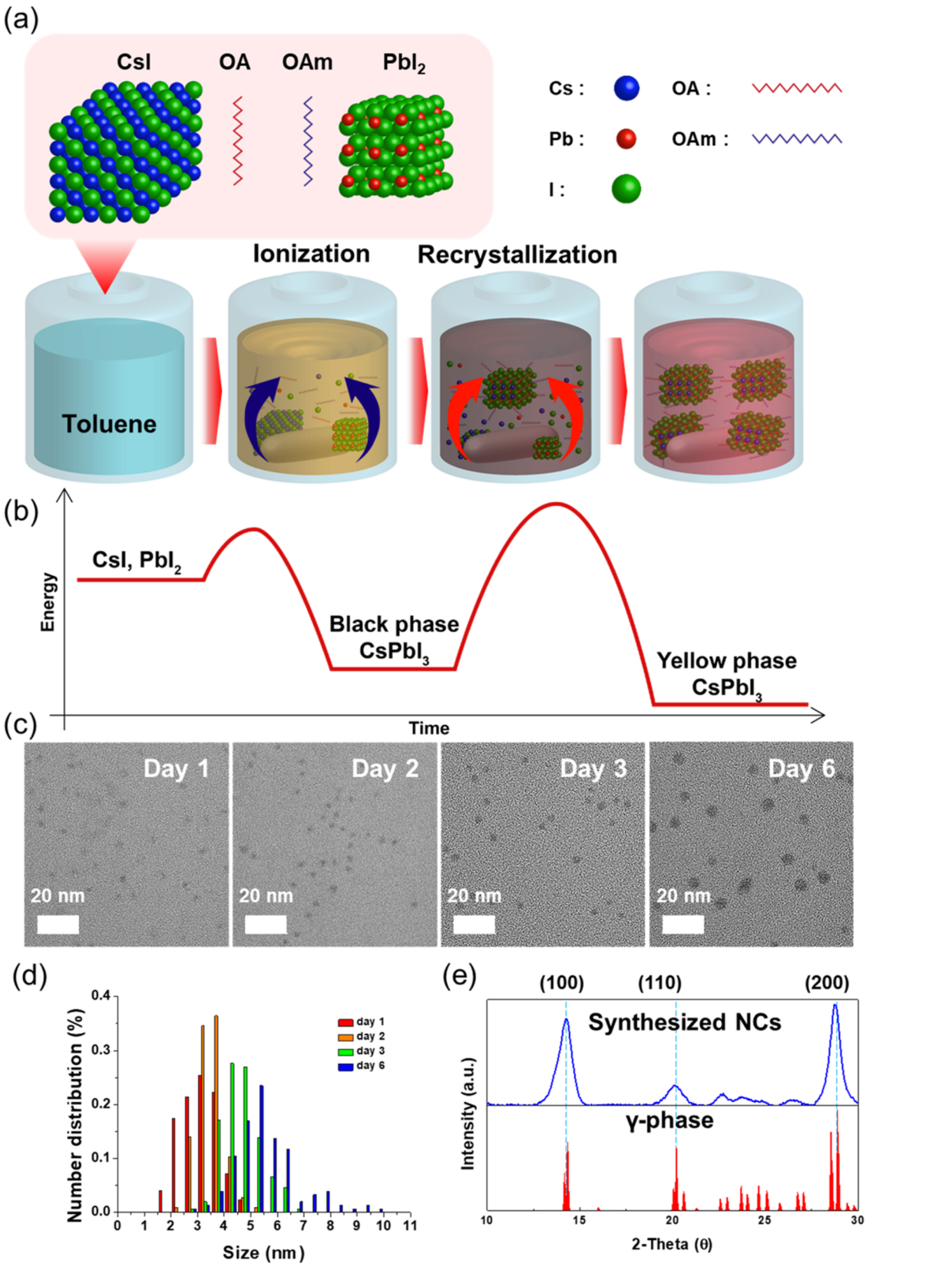

Figure 1. (a) Schematics of our new synthesis method. (b) Energy diagram based on phases of $CsPbI_3$ synthesized using CsI and PbI_2 in our room-temperature synthesis mechanism. (c) TEM images of nanoparticle size in the supernatant by synthesis time. (d) Number distribution by size of nanoparticles in the supernatant according to synthesis time. (e) Comparison of the XRD data of $CsPbI_3$ nanocrystals obtained 3 days after the start of synthesis with the γ-phase.

https://doi.org/10.1021/acsanm.4c04001
ACS Appl. Nano Mater. XXXX, XXX, XXX−XXX

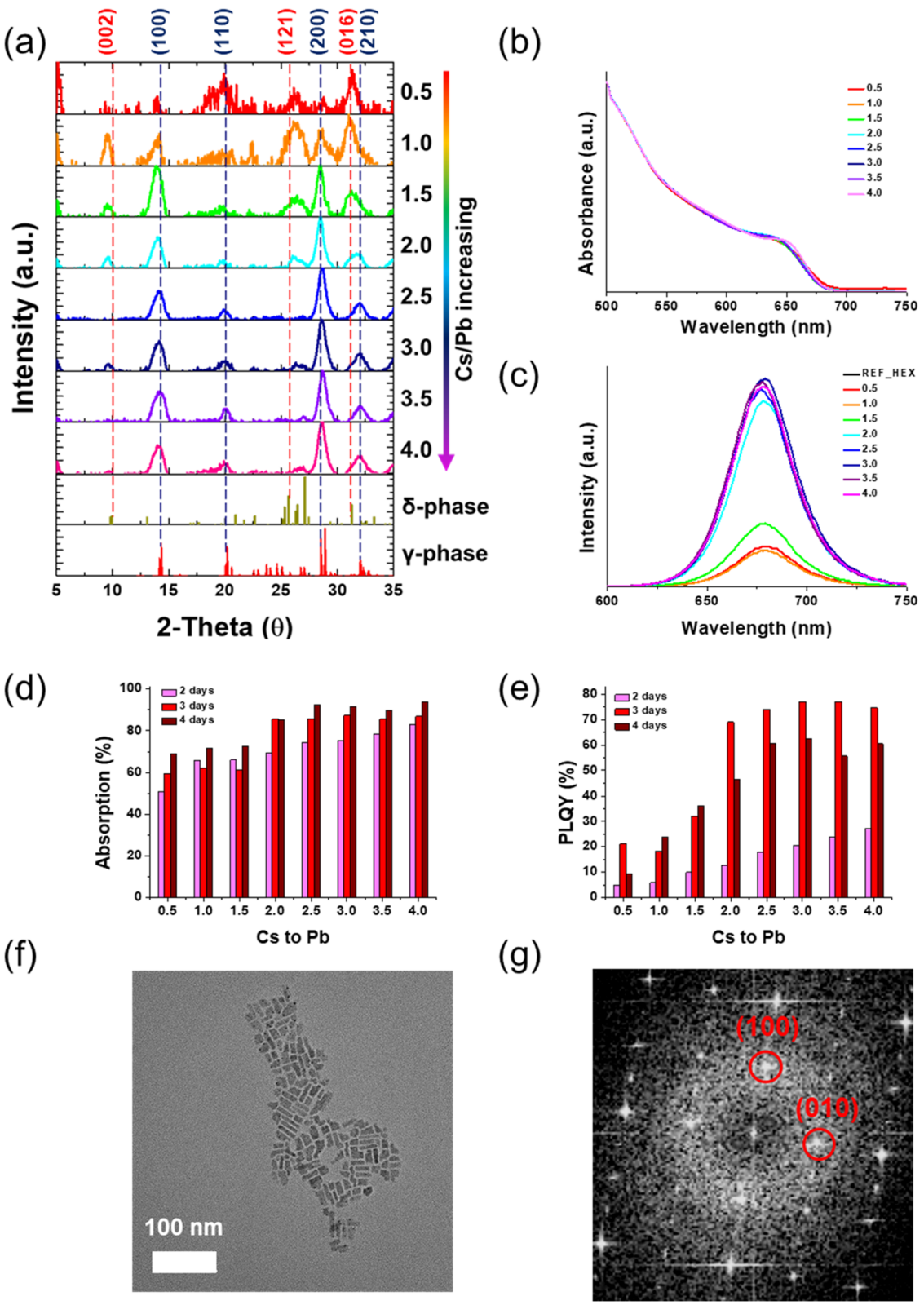

Figure 2. (a) XRD patterns, (b) UV−vis spectra, and (c) PL spectra of $CsPbI_3$ nanocrystals with different ratios of Cs to Pb. Comparisons of (d) absorptance and (e) PLQY according to synthesis time and Cs-to-Pb ratio under 380 nm excitation. (f) TEM image of synthesized $CsPbI_3$ IPNCs by our method. (g) FFT pattern for $CsPbI_3$ nanocrystal.

RESULTS AND DISCUSSION

Synthesis Mechanism. As shown in Figure 1a, we mixed CsI, PbI_2, toluene, oleic acid (OA), and oleylamine (OAm) in one pot and stirred the mixture. As synthesis progressed over time, ionization and recrystallization repeatedly occurred, leading to the synthesis of $CsPbI_3$ IPNCs. When synthesizing $CsPbBr_3$, we accelerated the synthesis rate by using a polar solvent. However, for $CsPbI_3$, adding a polar solvent like DMF

https://doi.org/10.1021/acsanm.4c04001
ACS Appl. Nano Mater. XXXX, XXX, XXX−XXX

or DMSO caused a phase transition to a yellow phase. Therefore, the synthesis was performed by excluding the polar solvent and adding only toluene and ligands. In our synthesis method, black-phase $CsPbI_3$ nanocrystals were synthesized first and then transformed to the yellow phase. Because the black phase is metastable at room temperature, it changed to the yellow phase when the synthesis time (referring to the time from the start of the synthesis) was prolonged (Figure 1b). However, using a polar solvent accelerates the phase transition from black phase to yellow phase. Therefore, a method was required to shorten the synthesis time without using a polar solvent. Without a polar solvent, ionization occurs slowly because of the low solubility of toluene and the added ligands. To increase the synthesis rate of the nanocrystals, we employed a method of increasing the amount of cesium ions to accelerate their growth rate. During the initial stage of synthesis, nanocrystals form through ion recrystallization, but due to the low ion concentration, very small $CsPbI_3$ nanocrystals are formed. Due to their small size, these nanocrystals are synthesized in the black phase, which is more stable than the yellow phase when the particle size of $CsPbI_3$ is on the order of several nanometers.[32]

We developed the synthesis process of our method by confirming that the size of the nanoparticles in the supernatant increased according to the synthesis time in TEM images (Figure 1c). Small nanoparticles were generated at the beginning of the synthesis, and then the nanoparticles gradually grew (Figure 1d). For $CsPbI_3$, the yellow phase is generally stable at room temperature, but when the particles are smaller than 5.6 nm, the black phase becomes stable. On the third day after the start of the synthesis, the average nanocrystal diameter was 4.63 nm, and on the sixth day, the average nanocrystal diameter was 6.05 nm. We confirmed that the nanocrystals synthesized over 3 days were in the black phase (Figure 1e).

Even if the nanoparticles grow with the synthesis time, the black phase could be maintained because the activation energy for the transition to the yellow phase is higher for nanoparticles compared to bulk. In the XRD pattern, the yellow phase increased from the fourth day of synthesis (Figure S1). As the size of the synthesized nanoparticles increased, the yellow phase became more stable, and the activation energy for phase transition decreased.

Wang et al. found that the phase transition to the yellow phase of $CsPbI_3$ can be suppressed using DBSA.[23] We experimented with adjusting the ratio of OA and DBSA to apply this method to our synthesis method. However, the addition of DBSA caused a redshift and hindered successful synthesis (Figure S2). Also, a significant decrease in PLQY occurred (Figure S3). Consequently, the use of DBSA in our synthesis method was not successful. Optimization of the achievable concentration based on changes in ligands seems necessary. Therefore, we proceeded with experiments using only OA and OAm as ligands.

During centrifugation, we attempted to prevent the transformation into the yellow phase when washing the ligands. Without removing the ligands, the surface becomes overly coated with ligands when the emissive layer (EML) is spin-coated, rendering it unsuitable for use in LEDs. When a small amount of isopropyl alcohol (IPA) was used during the washing process, a slight blueshift occurred, and there was no significant change in quantum efficiency (Figures S4 and S5). However, a significant quantity of ligands remained (Figure S6). We removed the ligands by mixing higher-density solvents into the synthesized solution to include the ligands in the supernatant. There were no differences in PL spectra, and some solvents exhibited an increase in PLQY (Figures S7 and S8). However, the ligands persisted and were not effectively removed (Figure S9).

Yang et al. identified cesium ions and oleylammonium as factors causing phase transformation.[36] Based on this method, we used a strategy in which ligands in the supernatant were removed through high-speed centrifugation, redispersion in the lightweight solvent (cyclohexane), and subsequent removal of residual compounds like cesium compounds at low-speed centrifugation. The washing step was then conducted by adding ethyl acetate. Consequently, it was possible to proceed with washing without a phase transformation into the yellow phase (Figures S10 and S11). The XRD peaks before and after the washing step appeared in similar positions (Figure S12). However, the peak for the (110) plane significantly decreased, and the peak position shifted slightly. This shift in peak position is due to the reduction in interplanar spacing caused by defects occurring as ligands were removed from the surface. As some surface ions were removed along with the ligands, the size of the nanocrystals slightly decreased, and the position of the peak shifted in the XRD spectrum.

Controlling Cs-to-Pb Ratio and Synthesis Time. We increased the amount of CsI to speed up the synthesis. During the synthesis of $CsPbI_3$, a higher amount of CsI allows cesium ions to more easily occupy the A site of the ABX_3 perovskite structure, promoting rapid nanoparticle formation. When the Cs-to-Pb ratio is relatively high (with more CsI), Pb vacancies occur, making the perovskite structure more stable.[37] However, if the rate of black-phase synthesis slows down compared to the rate of phase transition from black phase to yellow phase, the proportion of black phase decreases during synthesis. In the XRD pattern, the synthesis into the black phase improves more than the yellow phase as the ratio of Cs to Pb increases (Figure 2a). Furthermore, in the UV−vis and PL spectra, synthesized nanoparticles' absorption and emission peaks were the same regardless of the ratio of Cs to Pb (Figure 2b,c). However, in the XRD pattern, as the ratio of Cs to Pb increased, the ratio of the black phase increased, and the ratio of the yellow phase decreased (Figure 2a).

As the Cs-to-Pb ratio increases, we observed that the absorption of the nanocrystal solution also increases (Figure 2d). Absorption at a wavelength of 380 nm occurs in both the black and yellow phases. Therefore, the increase in absorption of the solution with increasing Cs-to-Pb ratio indicates the synthesis of more particles, implying an accelerated synthesis rate. Furthermore, it is observed that PLQY gradually increases as the Cs-to-Pb ratio increases, rather than remaining constant. Therefore, the ratio of Cs to Pb affects only the ratio of the black phase to the yellow phase, and the number of synthesized nanocrystals remains unchanged. When the Cs-to-Pb ratio was 2.0 or more, the synthesized IPNCs' XRD patterns and PL properties did not differ significantly (Figure 2a). Furthermore, the absorptance and PLQY of the synthesized $CsPbI_3$ nanocrystal solutions did not differ significantly at 2.0 or more of the Cs-to-Pb ratio (Figure 2d,e). Therefore, the Cs-to-Pb ratio was set to 3.0, which shows the maximum PLQY.

The results confirmed that the synthesis rate increased as the amount of Cs added increased, and a metastable black phase could be synthesized quickly (Figure 2d,e). In our results, although the synthesis rate of the nanocrystals increased, the phase transition rate from the black phase to the yellow phase was unaffected, resulting in the synthesis of $CsPbI_3$ nanocrystals containing a higher proportion of the black phase. This increase

https://doi.org/10.1021/acsanm.4c04001
ACS Appl. Nano Mater. XXXX, XXX, XXX−XXX

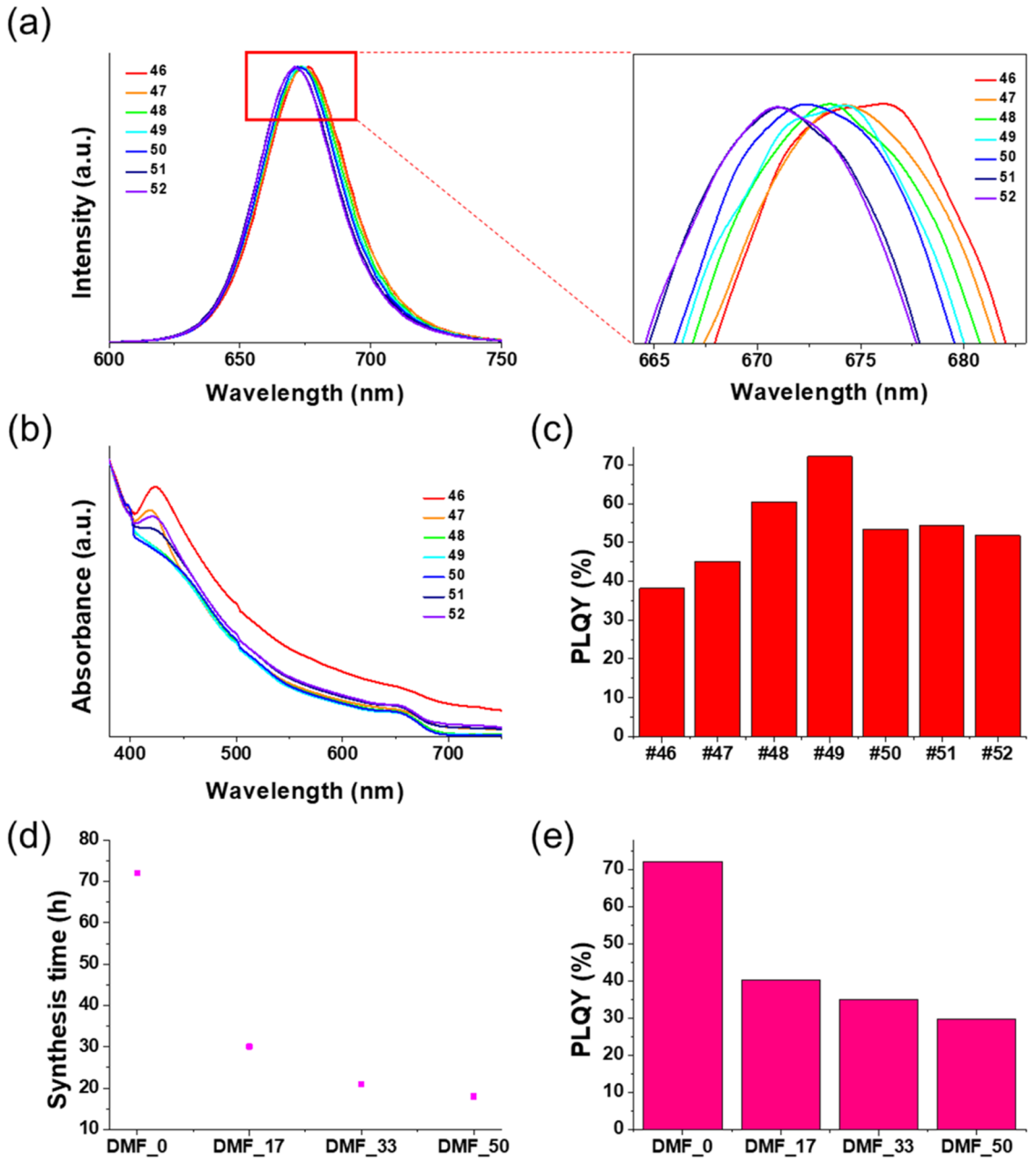

Figure 3. (a) PL spectra and (b) UV−vis spectra of $CsPbI_3$ nanocrystals prepared with different amounts of OAm (0.46, 0.47, 0.48, 0.49, 0.5, 0.51, and 0.52 mL per 10 mL toluene). (c) PLQY according to amounts of OAm under 380 nm excitation. (d) Synthesis time showing the maximum PLQY for $CsPbI_3$ nanocrystals according to different amounts of DMF added (0, 1.7, 3.3, and 5 μL DMF per 10 mL toluene). (e) PLQY according to amounts of DMF under 380 nm excitation.

in the black-phase ratio led to an improvement in PLQY. The absorption of the $CsPbI_3$ nanocrystal solutions increased with the synthesis time, so the number of synthesized nanocrystals increased with time (Figure 2d). However, PLQY was the highest on the third day of synthesis and decreased after that because the black phase changed to the yellow phase over time (Figure 2d,e). In the XRD pattern, the yellow phase increased from the fourth day of synthesis (Figure S1). On the fourth day of synthesis, we observed a phase transition from the black phase to the yellow phase. Consequently, on the third day of synthesis, a washing process was performed to remove ions, thereby inhibiting the further growth of nanoparticles.

At an excitation of 550 nm, there is almost no absorption by the yellow phase, so most of the absorption is due to the black phase. Therefore, the samples on the third day of synthesis had the highest photoluminescence external quantum efficiency (PL EQE) and absorption (Figure S13). Therefore, the black phase was synthesized first, and then the phase transitioned to the yellow phase; it is crucial to rapidly synthesize the black phase and delay the phase transition to the yellow phase. Consequently, an increase in the ratio of Cs to Pb increases the synthesis rate into the black phase and does not significantly affect the phase transition rate into the yellow phase. Therefore, we could obtain a $CsPbI_3$ nanocrystal solution with a higher PLQY of 78%.

The nanocrystals in the TEM image reveal a size of 10 nm on the short axis and 20 nm on the long axis (Figure 2f). The lattice parameter is measured as 0.6019 nm, consistent with the

https://doi.org/10.1021/acsanm.4c04001
ACS Appl. Nano Mater. XXXX, XXX, XXX−XXX

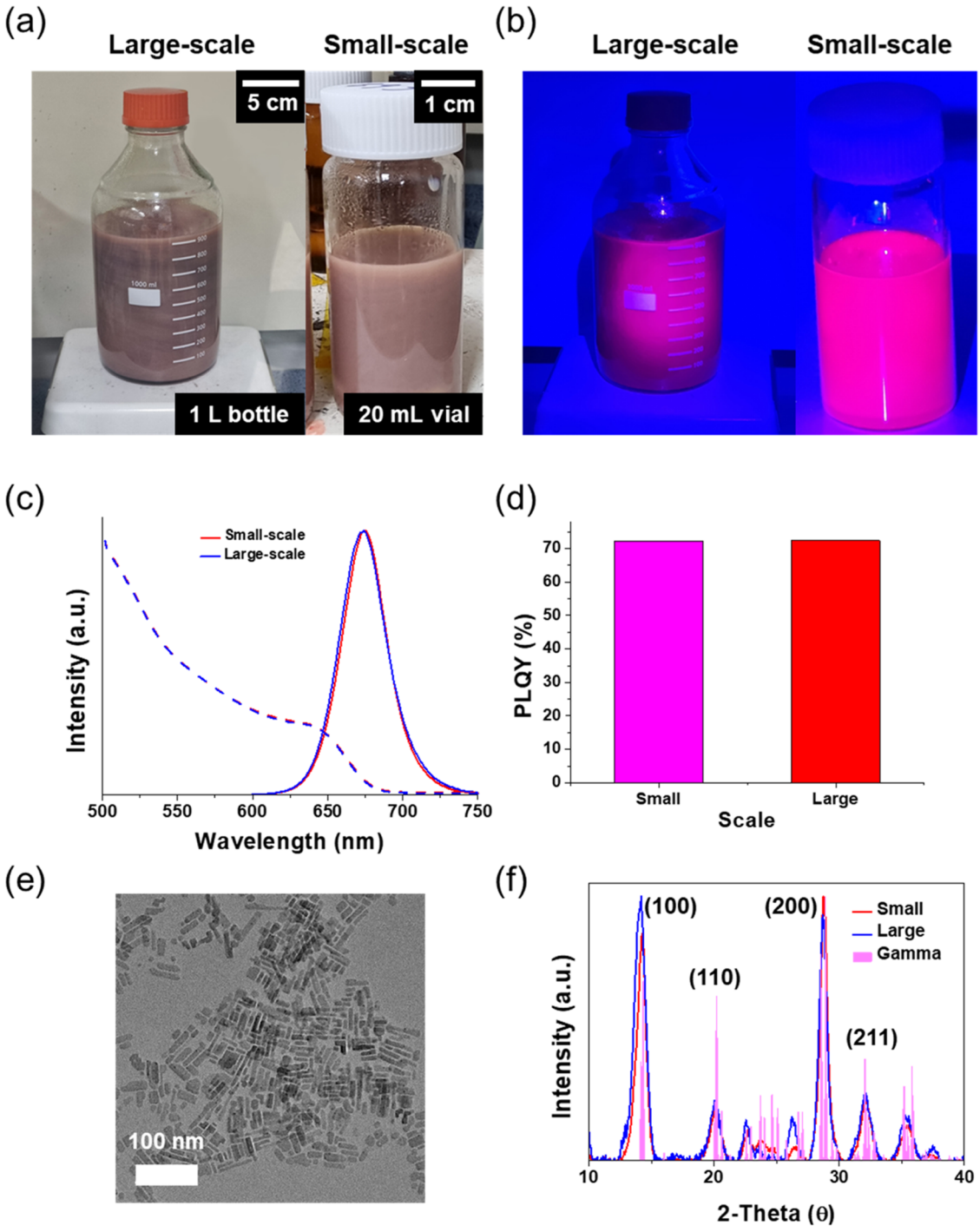

Figure 4. Images of large-scale (32 mmol, 1 L bottle) and small-scale (0.4 mmol, 20 mL vial) $CsPbI_3$ nanocrystal solutions (a) under room light and (b) UV light illumination. (c) UV−vis absorption and PL intensity comparison of large-scale and small-scale $CsPbI_3$ nanocrystal solutions. (d) PLQY comparison of $CsPbI_3$ nanocrystal solutions prepared by large-scale and small-scale synthesis. (e) TEM Image of synthesized $CsPbI_3$ IPNCs by large-scale synthesis. (f) XRD patterns of $CsPbI_3$ nanocrystals prepared with small-scale and large-scale synthesis.

orthorhombic structure's γ-phase parameter.[38] This result is the same in the XRD data (Figure 1e). Similarly, the FFT pattern of the TEM image reveals an orthorhombic structure (Figure 2g). Based on the FFT pattern, we obtained lattice parameters of 0.6024 and 0.6289 nm. These parameters also matched with the γ-phase $CsPbI_3$.[38] We measured the distance between dots in the FFT pattern and transformed it to 2θ degrees using eq 1. These 2θ values were matched with the γ-phase $CsPbI_3$ (Figure S14).

$$2\theta = 2\sin^{-1}(\lambda/2d) \quad (1)$$

In TEM images, particles in the black phase have sharp edges, while particles in the yellow phase have rounded edges (Figures S15 and S16). The interplanar distances for the black phase and the yellow phase were 0.31 and 0.24 nm, respectively, corresponding to the (200) and (200) interplanar distances of the γ-and δ-phases of $CsPbI_3$, respectively.

Controlling Oleylamine and DMF. We investigated the influence of the ratio of oleylammonium to cesium ions on

https://doi.org/10.1021/acsanm.4c04001
ACS Appl. Nano Mater. XXXX, XXX, XXX−XXX

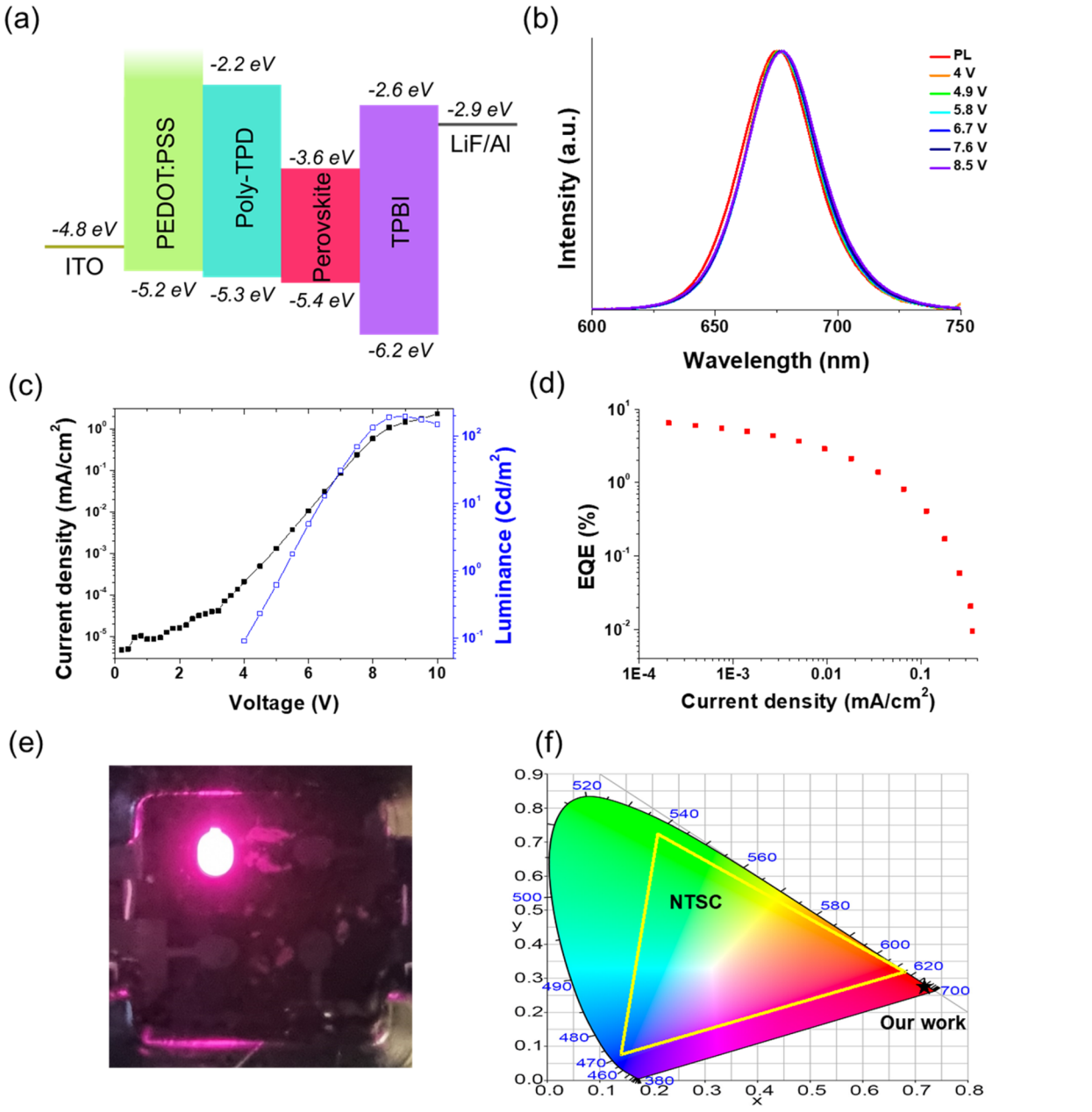

Figure 5. (a) Energy diagrams for the red LEDs. (b) EL spectra of the red LED by the applied voltage and PL spectrum of the $CsPbI_3$ solution. (c) *J*−*V*−*L* curve for the red LED (black squares indicate current density, and blue squares indicate luminance). (d) EQE versus current density of the red LED. (e) Images of red LEDs using large-scale synthesized $CsPbI_3$ nanocrystals. (f) CIE color coordinates corresponding to $CsPbI_3$ nanocrystals and NTSC standard.

nanocrystal synthesis by synthesizing the $CsPbI_3$ nanocrystals with different amounts of OAm. Cs ions typically occupy the A site of $CsPbI_3$, but on the surface, oleylammonium can also occupy this site. Therefore, competition occurs between the two ions. As the amount of oleylammonium increases relative to cesium ions, it becomes more difficult for the cesium ions to attach to the A site of $CsPbI_3$, resulting in slower synthesis and smaller nanocrystal size.[39] When the amount of oleylammonium decreases relative to cesium ions, cesium ions readily attach to the A site, resulting in faster synthesis and larger nanocrystal size. With our synthesis method, if the synthesis rate is slow, the black phase synthesis may not be completed, and a phase transition to the yellow phase may occur. If the synthesis rate is fast and the particle size increases, the phase transition to the yellow phase occurs more quickly.

Therefore, we attempted optimization of the amount of OAm. We adjusted the amount of OAm added from 0.46 to 0.52 mL per 10 mL of toluene, observing a PL peak at 671−676 nm (Figure 3a). An increase in the amount of OAm leads to a blueshift (Figure 3a) because the increase in oleylammonium relative to cesium ions resulted in slower synthesis and smaller nanocrystal formation. In the UV−vis spectra, we observed a 420 nm peak in some samples, indicating the presence of a yellow phase (Figure 3b). Therefore, if the amount of oleylamine added is larger or smaller than 0.49 mL per 10 mL of toluene, a yellow phase forms easily.

https://doi.org/10.1021/acsanm.4c04001
ACS Appl. Nano Mater. XXXX, XXX, XXX−XXX

When the black phase synthesis rate is slower than the phase transition rate into the yellow phase, the difference between the synthesis rate into the black phase and the phase transition rate into the yellow phase decreases, leading to a relatively higher proportion of the yellow phase. Conversely, if the synthesis rate increases, and the nanocrystal size grows over 5.6 nm, the phase transition rate into the yellow phase increases. Therefore, an optimal concentration of OAm exists. As shown in Figure 3c, the highest PLQY occurred when 0.49 mL of OAm was added per 10 mL of toluene.

We controlled the synthesis rate using a small amount of polar solvent in the large-scale synthesis method of blue perovskite nanocrystals we developed.[18] We used DMF to investigate whether we can control the synthesis rate using a polar solvent in the large-scale synthesis of red perovskite nanocrystals using $CsPbI_3$. Because black-phase $CsPbI_3$ transformed to the yellow phase from a polar solvent, we used a maximum of 5 μL of DMF per 10 mL of toluene. As the amount of DMF increased, the synthesis time for achieving maximum PLQY decreased (Figure 3d). However, the PLQY also decreased with the increase in DMF (Figure 3e). Using a polar solvent can increase the synthesis rate into the black phase, but it significantly accelerates the phase transition rate into the yellow phase. Therefore, for $CsPbI_3$ nanocrystals, there are limitations to using a polar solvent to achieve a faster synthesis rate.

Large-Scale Synthesis. In our synthesis method, small-scale synthesis (0.4 mmol) refers to ten times the typical laboratory synthesis unit (0.04 mmol or less), while large-scale synthesis (32 mmol) involves using 800 times the quantity of compounds typically used.[19,20] The large-scale synthesis was performed as shown in Figure 4a,b. Furthermore, the UV−vis and PL spectra of the synthesized nanocrystals did not differ between large-scale and small-scale synthesis (Figure 4c). The PLQYs of large-scale and small-scale synthesis were 72.3 and 72.1% (Figure 4d), respectively. We confirmed TEM images of $CsPbI_3$ nanocrystals synthesized through large-scale synthesis (Figure 4e). $CsPbI_3$ nanocrystals synthesized with large-scale synthesis were identical to those synthesized through small-scale synthesis (Figures 2f and 4e). The nanocrystal size was similar, and their rectangular shape was also consistent. Furthermore, we observed peaks appearing at the same positions when comparing XRD patterns (Figure 4f). Although there were slight differences in the intensity ratios, all of them matched the XRD pattern of the γ-$CsPbI_3$.

We added ZnI_2 solution to the synthesized $CsPbI_3$ solution for post-treatment in order to remove defects.[18,40,41] As a result of the post-treatment, the PLQY improved (Figure S17). For the post-treatment of the ZnI_2 solution, the PLQY improved as the amount of the solution increased. The surface defects were removed by the I^- in the ZnI_2 solution, resulting in an increase in PLQY. However, the PLQY did not continue to increase and saturated around 30 to 40 μL/mL. Furthermore, when a large amount of the post-treatment solution is added, ligands and ions are increased in the $CsPbI_3$ solution, so $CsPbI_3$ nanocrystals easily change to a yellow phase. This occurs because the ligands enhance solubility and the residual ions promote nanocrystal growth, which lowers the activation energy required for the phase transition. As a result, the $CsPbI_3$ nanocrystals transform into the yellow phase. When post-treated with a $ZnBr_2$ solution, the synthesized $CsPbI_3$ nanocrystals undergo halide ion exchange, leading to the blueshift (Figure S18).

Fabrication of Red LED. We fabricated a red LED using the synthesized $CsPbI_3$ nanocrystals, which were synthesized on a large scale, and the LED structure was configured as shown in Figure 5a. We fabricated red LEDs with a $CsPbI_3$ solution post-treated at a concentration of 20 μL/mL with a ZnI_2 solution. The position of the PL peak in the solution state and the EL peak when fabricated as a red LED were shifted 1 nm (Figure 5b). Furthermore, a stable peak position and fwhm were shown even when the voltage was increased. The EL peak position was 675 nm, and the fwhm was 33 nm. The fabricated red LED's external quantum efficiency (EQE) was 6.4%, and the maximum luminescence was 204 cd/m^2 (Figure 5c,d). In addition, we confirmed that the LEDs fabricated with $CsPbI_3$ synthesized on a small scale showed similar performance to those fabricated with $CsPbI_3$ synthesized on a large scale (Figure S19). As shown in Figure 5e, the LED we fabricated emits red light. The red LED we fabricated emitted a color outside the National Television Standard Committee (NTSC) color triangle on the CIE color coordinates (Figure 5f).

LEDs fabricated using $CsPbI_3$ nanocrystals without ZnI_2 post-treatment exhibited a broad peak near 420 nm, corresponding to the EL spectrum of poly-TPD (Figure S20). However, as the applied voltage increased, an emission peak at 675 nm, corresponding to the EL peak of the emitting layer composed of $CsPbI_3$ nanocrystals, was observed. This phenomenon is attributed to the significantly slower hole injection rate compared to the electron injection rate. With increasing voltage, hole injection from the HTL to the emitting layer improved, resulting in the occurrence of the EL peak from the emitting layer.

To address this issue, the $CsPbI_3$ solution was post-treated with a ZnI_2 solution. LEDs post-treated with 40 μL/mL of ZnI_2 solution did not exhibit the EL spectrum of poly-TPD. The post-treatment solution contained ZnI_2 and OAm. During the post-treatment process, defects in the $CsPbI_3$ layer were passivated, and the concentration of OAm increased (Figure S17). Consequently, defect passivation enhanced light emission from the $CsPbI_3$ layer, while the increased ligand concentration reduced conductivity, thereby decreasing electron mobility.

We confirmed the current density according to the concentration of post-treatment ZnI_2 solution (Figure S21). The concentration of the ZnI_2 solution was increased, and the current density was decreased because ligands containing the ZnI_2 solution hindered current flow. Additionally, electron injection into the emitting layer was suppressed to achieve charge balance between electrons and holes. This shift caused exciton recombination, previously occurring in the HTL, to relocate to the emitting layer, leading to the emergence of the emission peak from $CsPbI_3$. However, the increased ligand concentration reduced conductivity and charge injection efficiency. As a result, at ZnI_2 solution concentrations exceeding 40 μL/mL, the luminescence dropped to approximately 1 cd/m^2, highlighting a trade-off between defect passivation and charge transport in the system.

Therefore, in LEDs without post-treated with ZnI_2 solution, recombination of excitons occurred in the poly-TPD layer. In LEDs post-treated with ZnI_2 solution, the recombination of excitons occurred in the $CsPbI_3$ layer because ligands hindered electron mobility at the $CsPbI_3$ layer. The luminescence of $CsPbI_3$ LEDs was highest when post-treated with 20 μL/mL of ZnI_2 solution (Figure S22). LEDs fabricated using $CsPbI_3$ nanocrystals without ZnI_2 post-treatment had low luminescence because of recombination in the poly-TPD layer. LEDs post-treated with 40 μL/mL of ZnI_2 solution exhibited low luminance and EQE caused by the high concentration of ligands.

https://doi.org/10.1021/acsanm.4c04001
ACS Appl. Nano Mater. XXXX, XXX, XXX−XXX

$CsPbI_3$ NCs have a large surface-to-volume ratio, resulting in a high content of organic ligands, which leads to low electrical conductivity. To improve the EQE of the fabricated LED, it is necessary to optimize the device structure to promote electron−hole recombination in the emitting layer, improve the conductivity of the emitting layer by modifying the ligands, and ensure efficient charge injection from both the HTL and ETL into the emitting layer. Enhancing charge injection will facilitate balanced carrier dynamics, enabling more effective exciton formation and light emission in the desired region.

These results demonstrated that $CsPbI_3$ nanocrystals can be mass-synthesized at room temperature and synthesized into perovskite structures exhibiting light-emitting properties that can be applied to LEDs.

CONCLUSIONS

In this study, we developed a large-scale synthesis of black-phase $CsPbI_3$ nanocrystals at room temperature in ambient conditions. We synthesized the same nanocrystals regardless of the synthesized amount, and the PL peak appeared at approximately 670 nm. PLQY of $CsPbI_3$ nanocrystals synthesized by our method increased from 72 to 78% after post-treatment with ZnI_2 solution. The synthesis rate changed according to the Cs-to-Pb ratio—the more Cs, the faster the synthesis rate, but saturated above a specific ratio. We controlled the amount of OAm and obtained the optimum amount. We have developed a new synthesis method for $CsPbI_3$ nanocrystals. With this method, we synthesized 32 mmol in a single batch, which is more than 800 times the quantity synthesized by conventional methods using 0.04 mmol or less. Moreover, the synthesis method is cost-effective for large-scale production, as it occurs in one step at room temperature. While there have been other studies on large-scale synthesis, none have attempted one-pot, one-step synthesis at room temperature under ambient conditions. In our research, we have developed an economically feasible large-scale synthesis technology for the commercialization of $CsPbI_3$ nanocrystals by creating conditions for homogeneous synthesis reactions and stable existence of γ-$CsPbI_3$ at room temperature.

We fabricated red LEDs using $CsPbI_3$ nanocrystals. The EL peak was 1 nm red-shifted compared with the PL peak, and the red LED had an EQE of 6.4%. Despite current issues with low conductivity in the HTL, we achieved stable recombination in the EML by modifying the surface ligands. However, improving the conductivity of the HTL could enable the fabrication of higher-performance LEDs with fewer ligands on the $CsPbI_3$ nanocrystals. Additionally, adjusting the type and ratio of ligands during synthesis to form a cubic structure instead of a plate structure would reduce the surface-to-volume ratio, thereby improving conductivity. The red LED showed the maximum EL of 204 cd/m^2, which is low. To date, the maximum EL reported in studies fabricating red LEDs with $CsPbI_3$ IPNCs synthesized at room temperature also appears to be around 200 cd/m^2.[10,23] Hence, research is necessary to increase the luminance of LEDs fabricated with $CsPbI_3$ synthesized at ambient conditions. This research will significantly help the commercial use of inorganic perovskites-based LEDs.

ASSOCIATED CONTENT

Supporting Information

The Supporting Information is available free of charge at https://pubs.acs.org/doi/10.1021/acsanm.4c04001.

The PL properties of synthesized NPLs according to each variable. The additional TEM, XRD, and PL spectra data. The figure that explanation for stacked NPLs making additional XRD peaks (PDF)

AUTHOR INFORMATION

Corresponding Author

Jin-Woo Park − *Department of Materials Science and Engineering, Yonsei University, Seoul 03722, Republic of Korea;* orcid.org/0000-0003-0965-373X; Phone: +82-221235834; Email: jwpark09@yonsei.ac.kr

Authors

Ju-Hyun Yoo − *Department of Materials Science and Engineering, Yonsei University, Seoul 03722, Republic of Korea*

Kyung Yeon Jang − *Department of Materials Science and Engineering, Seoul National University, Seoul 08826, Republic of Korea*

Jihye Jang − *Department of Materials Science and Engineering, Yonsei University, Seoul 03722, Republic of Korea*

Cheolmin Park − *Department of Materials Science and Engineering, Yonsei University, Seoul 03722, Republic of Korea;* orcid.org/0000-0002-6832-0284

Tae-Woo Lee − *Department of Materials Science and Engineering, Seoul National University, Seoul 08826, Republic of Korea; School of Chemical and Biological Engineering, Institute of Engineering Research, Research Institute of Advanced Materials, Soft Foundry, Seoul National University, Seoul 08826, Republic of Korea;* orcid.org/0000-0002-6449-6725

Complete contact information is available at: https://pubs.acs.org/10.1021/acsanm.4c04001

Notes

The authors declare no competing financial interest.

ACKNOWLEDGMENTS

This work was supported by the National Research Foundation of Korea (NRF) grant funded by the Korean government (MSIT) (No. RS-2023-00302611).

REFERENCES

(1) Beal, R. E.; Slotcavage, D. J.; Leijtens, T.; Bowring, A. R.; Belisle, R. A.; Nguyen, W. H.; Burkhard, G. F.; Hoke, E. T.; McGehee, M. D. Cesium Lead Halide Perovskites with Improved Stability for Tandem Solar Cells. *J. Phys. Chem. Lett.* **2016**, *7* (5), 746−751.

(2) Xu, X.; Zhang, H.; Li, E.; Ru, P.; Chen, H.; Chen, Z.; Wu, Y.; Tian, H.; Zhu, W. H. Electron-enriched thione enables strong Pb-S interaction for stabilizing high quality CsPbI3 perovskite films with low-temperature processing. *Chem. Sci.* **2020**, *11* (12), 3132−3140.

(3) Song, J.; Xu, L.; Li, J.; Xue, J.; Dong, Y.; Li, X.; Zeng, H. Monolayer and Few-Layer All-Inorganic Perovskites as a New Family of Two-Dimensional Semiconductors for Printable Optoelectronic Devices. *Adv. Mater.* **2016**, *28* (24), 4861−4869.

(4) Akbulatov, A. F.; Luchkin, S. Y.; Frolova, L. A.; Dremova, N. N.; Gerasimov, K. L.; Zhidkov, I. S.; Anokhin, D. V.; Kurmaev, E. Z.; Stevenson, K. J.; Troshin, P. A. Probing the Intrinsic Thermal and Photochemical Stability of Hybrid and Inorganic Lead Halide Perovskites. *J. Phys. Chem. Lett.* **2017**, *8* (6), 1211−1218.

(5) Zhang, L.; Yang, X.; Jiang, Q.; Wang, P.; Yin, Z.; Zhang, X.; Tan, H.; Yang, Y. M.; Wei, M.; Sutherland, B. R.; Sargent, E. H.; You, J. Ultra-bright and highly efficient inorganic based perovskite light-emitting diodes. *Nat. Commun.* **2017**, *8*, No. 15640.

(6) Li, G.; Rivarola, F. W.; Davis, N. J.; Bai, S.; Jellicoe, T. C.; de la Pena, F.; Hou, S.; Ducati, C.; Gao, F.; Friend, R. H.; Greenham, N. C.; Tan, Z. K. Highly Efficient Perovskite Nanocrystal Light-Emitting Diodes Enabled by a Universal Crosslinking Method. *Adv. Mater.* **2016**, *28* (18), 3528−3534.
(7) Pan, J.; Quan, L. N.; Zhao, Y.; Peng, W.; Murali, B.; Sarmah, S. P.; Yuan, M.; Sinatra, L.; Alyami, N. M.; Liu, J.; Yassitepe, E.; Yang, Z.; Voznyy, O.; Comin, R.; Hedhili, M. N.; Mohammed, O. F.; Lu, Z. H.; Kim, D. H.; Sargent, E. H.; Bakr, O. M. Highly Efficient Perovskite-Quantum-Dot Light-Emitting Diodes by Surface Engineering. *Adv. Mater.* **2016**, *28* (39), 8718−8725.
(8) Song, J.; Li, J.; Xu, L.; Li, J.; Zhang, F.; Han, B.; Shan, Q.; Zeng, H. Room-Temperature Triple-Ligand Surface Engineering Synergistically Boosts Ink Stability, Recombination Dynamics, and Charge Injection toward EQE-11.6% Perovskite QLEDs. *Adv. Mater.* **2018**, *30* (30), No. e1800764.
(9) Huang, H.; Li, Y.; Tong, Y.; Yao, E. P.; Feil, M. W.; Richter, A. F.; Doblinger, M.; Rogach, A. L.; Feldmann, J.; Polavarapu, L. Spontaneous Crystallization of Perovskite Nanocrystals in Nonpolar Organic Solvents: A Versatile Approach for their Shape-Controlled Synthesis. *Angew. Chem., Int. Ed.* **2019**, *58* (46), 16558−16562.
(10) Han, B. N.; Cai, B.; Shan, Q. S.; Song, J. Z.; Li, J. H.; Zhang, F. J.; Chen, J. W.; Fang, T.; Ji, Q. M.; Xu, X. B.; Zeng, H. Stable, Efficient Red Perovskite Light-Emitting Diodes by (α, δ)-CsPbI3 Phase Engineering. *Adv. Funct. Mater.* **2018**, *28* (47), No. 1804285.
(11) Min, X. H.; Xie, Q. F.; Wang, X. Z.; Chen, M. X. Enhancing the stability of cesium lead iodide perovskite nanocrystals: Recent progress, challenges and opportunities. *Surf. Interfaces* **2021**, *22*, No. 100870.
(12) Zhu, P.; Thapa, S.; Zhu, H.; Venugopal, D.; Sambou, A.; Yue, Y.; Dantuluri, S. S.; Gangopadhyay, S. Solid-State White Light-Emitting Diodes Based on 3D-Printed CsPbX3-Resin Color Conversion Layers. *ACS Appl. Electron. Mater.* **2023**, *5* (10), 5316−5324.
(13) Pathak, S.; Sakai, N.; Rivarola, F. W. R.; Stranks, S. D.; Liu, J. W.; Eperon, G. E.; Ducati, C.; Wojciechowski, K.; Griffiths, J. T.; Haghighirad, A. A.; Pellaroque, A.; Friend, R. H.; Snaith, H. J. Perovskite Crystals for Tunable White Light Emission. *Chem. Mater.* **2015**, *27* (23), 8066−8075.
(14) Dutta, A.; Dutta, S. K.; Das Adhikari, S.; Pradhan, N. Phase-Stable CsPbI3 Nanocrystals: The Reaction Temperature Matters. *Angew. Chem., Int. Ed.* **2018**, *57* (29), 9083−9087.
(15) Song, J.; Li, J.; Li, X.; Xu, L.; Dong, Y.; Zeng, H. Quantum Dot Light-Emitting Diodes Based on Inorganic Perovskite Cesium Lead Halides (CsPbX3). *Adv. Mater.* **2015**, *27* (44), 7162−7167.
(16) Dai, L.; Deng, Z.; Auras, F.; Goodwin, H.; Zhang, Z.; Walmsley, J. C.; Bristowe, P. D.; Deschler, F.; Greenham, N. C. Slow carrier relaxation in tin-based perovskite nanocrystals. *Nat. Photonics* **2021**, *15* (9), 696−702.
(17) Han, T.-H.; Jang, K. Y.; Dong, Y.; Friend, R. H.; Sargent, E. H.; Lee, T.-W. A roadmap for the commercialization of perovskite light emitters. *Nat. Rev. Mater.* **2022**, *7* (10), 757−777.
(18) Yoo, J. H.; Kim, S.; Lee, H.; Park, C.; Lee, T. W.; Park, J. W. Room-Temperature, Homogeneous, Single-Step, and Large-Scale Synthesis of Perovskite Nanoplatelets for Blue Light-Emitting Diodes. *ACS Appl. Mater. Interfaces* **2023**, *15* (33), 39461−39471.
(19) Protesescu, L.; Yakunin, S.; Bodnarchuk, M. I.; Krieg, F.; Caputo, R.; Hendon, C. H.; Yang, R. X.; Walsh, A.; Kovalenko, M. V. Nanocrystals of Cesium Lead Halide Perovskites (CsPbX3, X = Cl, Br, and I): Novel Optoelectronic Materials Showing Bright Emission with Wide Color Gamut. *Nano Lett.* **2015**, *15* (6), 3692−3696.
(20) Li, X. M.; Wu, Y.; Zhang, S. L.; Cai, B.; Gu, Y.; Song, J. Z.; Zeng, H. B. CsPbX3 Quantum Dots for Lighting and Displays: Room-Temperature Synthesis, Photoluminescence Superiorities, Underlying Origins and White Light-Emitting Diodes. *Adv. Funct. Mater.* **2016**, *26* (15), 2435−2445.
(21) Bohn, B. J.; Tong, Y.; Gramlich, M.; Lai, M. L.; Doblinger, M.; Wang, K.; Hoye, R. L. Z.; Muller-Buschbaum, P.; Stranks, S. D.; Urban, A. S.; Polavarapu, L.; Feldmann, J. Boosting Tunable Blue Luminescence of Halide Perovskite Nanoplatelets through Postsynthetic Surface Trap Repair. *Nano Lett.* **2018**, *18* (8), 5231−5238.
(22) Yin, W. X.; Li, M. K.; Dong, W.; Luo, Z.; Li, Y. X.; Qan, J. Y.; Zhang, J. Q.; Zhang, W.; Zhang, Y.; Kershaw, S. V.; Zhang, X. Y.; Zheng, W. T.; Rogach, A. L. Multidentate Ligand Polyethylenimine Enables Bright Color-Saturated Blue Light-Emitting Diodes Based on CsPbBr3 Nanoplatelets. *ACS Energy Lett.* **2021**, *6* (2), 477−484.
(23) Wang, T. T.; Li, X. S.; Fang, T.; Wang, S. L.; Song, J. Z. Room-temperature synthesis of perovskite-phase CsPbI3 nanocrystals for optoelectronics via a ligand-mediated strategy. *Chem. Eng. J.* **2021**, *418*, No. 129361.
(24) Wang, B.; Novendra, N.; Navrotsky, A. Energetics, Structures, and Phase Transitions of Cubic and Orthorhombic Cesium Lead Iodide (CsPbI3) Polymorphs. *J. Am. Chem. Soc.* **2019**, *141* (37), 14501−14504.
(25) Dastidar, S.; Egger, D. A.; Tan, L. Z.; Cromer, S. B.; Dillon, A. D.; Liu, S.; Kronik, L.; Rappe, A. M.; Fafarman, A. T. High Chloride Doping Levels Stabilize the Perovskite Phase of Cesium Lead Iodide. *Nano Lett.* **2016**, *16* (6), 3563−3570.
(26) Dastidar, S.; Hawley, C. J.; Dillon, A. D.; Gutierrez-Perez, A. D.; Spanier, J. E.; Fafarman, A. T. Quantitative Phase-Change Thermodynamics and Metastability of Perovskite-Phase Cesium Lead Iodide. *J. Phys. Chem. Lett.* **2017**, *8* (6), 1278−1282.
(27) Sutton, R. J.; Eperon, G. E.; Miranda, L.; Parrott, E. S.; Kamino, B. A.; Patel, J. B.; Hörantner, M. T.; Johnston, M. B.; Haghighirad, A. A.; Moore, D. T.; Snaith, H. J. Bandgap-Tunable Cesium Lead Halide Perovskites with High Thermal Stability for Efficient Solar Cells. *Adv. Energy Mater.* **2016**, *6* (8), No. 1502458.
(28) Lan, J. Z.; Luo, L.; Wang, M. M.; Li, F.; Wu, X. X.; Wang, F. One pot gram-scale synthesis of CsPbBr3 nanocrystals and their application in green LED. *J. Lumin.* **2019**, *210*, 464−471.
(29) Zhang, F.; Zhong, H.; Chen, C.; Wu, X. G.; Hu, X.; Huang, H.; Han, J.; Zou, B.; Dong, Y. Brightly Luminescent and Color-Tunable Colloidal CH3NH3PbX3 (X = Br, I, Cl) Quantum Dots: Potential Alternatives for Display Technology. *ACS Nano* **2015**, *9* (4), 4533−4542.
(30) Huang, H.; Zhao, F.; Liu, L.; Zhang, F.; Wu, X. G.; Shi, L.; Zou, B.; Pei, Q.; Zhong, H. Emulsion Synthesis of Size-Tunable CH3NH3PbBr3 Quantum Dots: An Alternative Route toward Efficient Light-Emitting Diodes. *ACS Appl. Mater. Interfaces* **2015**, *7* (51), 28128−28133.
(31) Eperon, G. E.; Paternò, G. M.; Sutton, R. J.; Zampetti, A.; Haghighirad, A. A.; Cacialli, F.; Snaith, H. J. Inorganic caesium lead iodide perovskite solar cells. *J. Mater. Chem. A* **2015**, *3* (39), 19688−19695.
(32) Yang, R. X.; Tan, L. Z. Understanding size dependence of phase stability and band gap in CsPbI3 perovskite nanocrystals. *J. Chem. Phys.* **2020**, *152* (3), No. 034702.
(33) Kong, X. Q.; Shayan, K.; Hua, S.; Strauf, S.; Lee, S. S. Complete Suppression of Detrimental Polymorph Transitions in All-Inorganic Perovskites via Nanoconfinement. *ACS Appl. Energy Mater.* **2019**, *2* (4), 2948−2955.
(34) Masi, S.; Gualdrón-Reyes, A. F.; Mora-Seró, I. Stabilization of Black Perovskite Phase in FAPbI3 and CsPbI3. *ACS Energy Lett.* **2020**, *5* (6), 1974−1985.
(35) Becker, P.; Márquez, J. A.; Just, J.; Al-Ashouri, A.; Hages, C.; Hempel, H.; Jost, M.; Albrecht, S.; Frahm, R.; Unold, T. Low Temperature Synthesis of Stable γ-CsPbI3 Perovskite Layers for Solar Cells Obtained by High Throughput Experimentation. *Adv. Energy Mater.* **2019**, *9* (22), No. 1900555.
(36) Yang, H. S.; Suh, E. H.; Noh, S. H.; Jung, J.; Oh, J. G.; Lee, K. H.; Lee, D.; Jang, J. Facile low-energy and high-yield synthesis of stable α-CsPbI3 perovskite quantum dots: Decomposition mechanisms and solar cell applications. *Chem. Eng. J.* **2023**, *454*, No. 140331.
(37) Kye, Y.-H.; Yu, C.-J.; Jong, U.-G.; Ri, K.-C.; Kim, J.-S.; Choe, S.-H.; Hong, S.-N.; Li, S.; Wilson, J. N.; Walsh, A. Vacancy-Driven Stabilization of the Cubic Perovskite Polymorph of CsPbI3. *J. Phys. Chem. C* **2019**, *123* (15), 9735−9744.
(38) Marronnier, A.; Roma, G.; Boyer-Richard, S.; Pedesseau, L.; Jancu, J. M.; Bonnassieux, Y.; Katan, C.; Stoumpos, C. C.; Kanatzidis, M. G.; Even, J. Anharmonicity and Disorder in the Black Phases of

https://doi.org/10.1021/acsanm.4c04001
ACS Appl. Nano Mater. XXXX, XXX, XXX−XXX

Cesium Lead Iodide Used for Stable Inorganic Perovskite Solar Cells. *ACS Nano* **2018**, *12* (4), 3477−3486.
(39) Antami, K.; Bateni, F.; Ramezani, M.; Hauke, C. E.; Castellano, F. N.; Abolhasani, M. CsPbI3 Nanocrystals Go with the Flow: From Formation Mechanism to Continuous Nanomanufacturing. *Adv. Funct. Mater.* **2022**, *32* (6), No. 2108687.
(40) Li, F.; Liu, Y.; Wang, H.; Zhan, Q.; Liu, Q.; Xia, Z. Postsynthetic Surface Trap Removal of CsPbX3 (X = Cl, Br, or I) Quantum Dots via a ZnX2/Hexane Solution toward an Enhanced Luminescence Quantum Yield. *Chem. Mater.* **2018**, *30* (23), 8546−8554.
(41) Thapa, S.; Zhu, H.; Grigoriev, A.; Zhu, P. Novel Composite of Nickel Thiocyanate-Based All-Inorganic Lead Bromide Perovskite Nanocrystals with Enhanced Luminescent and Stability for White Light-Emitting Diodes. *Adv. Mater. Interfaces* **2022**, *9* (24), No. 2200710.

https://doi.org/10.1021/acsanm.4c04001
ACS Appl. Nano Mater. XXXX, XXX, XXX−XXX